Appl. Phys. B 83, 37–42 (2006)
DOI: 10.1007/s00340-006-2138-9

Applied Physics B
Lasers and Optics

D. TÜRKE[1,✉]
W. WOHLLEBEN[3]
J. TEIPEL[1]
M. MOTZKUS[3]
B. KIBLER[4]
J. DUDLEY[4]
H. GIESSEN[1,2]

Chirp-controlled soliton fission in tapered optical fibers

[1] Institut für Angewandte Physik, Universität Bonn, Wegelerstrasse 8, 53115 Bonn, Germany
[2] 4. Physikalisches Institut, Universität Stuttgart, Pfaffenwaldring 57, 70550 Stuttgart, Germany
[3] Institut für Physikalische Chemie, Philipps-Universität Marburg, Hans-Meerwein-Strasse, 35043 Marburg, Germany
[4] Insitut FEMTO-ST, Département d'Optique P-M Duffieux, Université de Franche-Comté, Besançon, France

Received: 26 October 2005/
Revised version: 22 December 2005
Published online: 10 February 2006 • © Springer-Verlag 2006

ABSTRACT Manipulation of the input pulse chirp during supercontinuum generation in tapered fibers provides precise control of the soliton fission process taking place in the taper waist. Simulations and experiments demonstrate that controlling this pre-chirp by a pulse shaper can be applied to compensate for deleterious effects due to untapered fiber pigtails. Temporal and cross-correlation frequency resolved measurements are utilized to show, that the control of the soliton fission dynamics can be obtained by manipulating the input pulse chirp through the imposition of a quadratic spectral phase.

PACS 42.65.Wi; 42.65.Tg; 42.81.Qb; 42.81.DP

1 Introduction

Although supercontinuum (SC) generation in photonic crystal fibers (PCF) and fiber tapers has now been intensively researched by many groups [1], the study of the SC evolution dynamics continues to be a subject of intense interest. For SC generation in PCF, considerable theoretical progress has been made, and the roles of soliton fission, parametric processes, and the influence of input pulse noise have been quantified [2, 3]. This has subsequently allowed the careful design of experiments that have generated SC with stability and bandwidth characteristics optimized for applications such as optical frequency metrology [4, 5] or pulse compression [6, 7]. Recent experiments have also focused on developing a more flexible approach to generating tailored SC using the adaptive manipulation of the input pulse intensity and phase to influence the precise manner in which the SC spectrum develops during propagation [8].

The majority of these previous studies have focused on pulse propagation in PCF, where the confinement and dispersion properties are constant along the interaction length. However, it has been known since the pioneering work of Birks et al. that, for SC generation applications, optical fiber tapers exhibit comparable nonlinearity enhancement and an equivalent freedom in dispersion control through modification of the taper cross-section [9]. Further studies have revealed the influence of the taper region [10]. Moreover, the fabrication of sub-wavelength tapers or "photonic wires" has recently led to extremely impressive results in ultra-low threshold SC generation [11]. In their waist regions, fiber tapers present comparable characteristics to those of high air-fill fraction PCF. However, the necessary presence of input and output standard fiber pigtail segments in realistic tapers significantly alters the SC generation dynamics. To our knowledge, however, this has not been the subject of any detailed study.

The objective of this paper is to examine this problem in detail, using simulations and experiment to provide insight into the SC evolution process in the different segments of a realistic tapered fiber, and to examine the effect of input pulse pre-chirp on the SC evolution process. Our major finding is that appropriate pre-chirping yields convenient control of the soliton fission process along the length of the taper and can compensate for deleterious effects due to propagation in the untapered input pigtail segment. We introduce a novel cartographic approach to represent the SC generation as a function of pre-chirp that facilitates convenient comparison between simulation and experiment, and we also report cross-correlation frequency resolved optical gating (XFROG) [17, 18] experiments on the SC characteristics as a function of pre-chirp.

2 Numerical simulations

Our simulations use a generalized nonlinear envelope equation model that has previously been shown to successfully describe the SC generation process over a wide parameter range [3, 4]. The model is based on a generalized scalar propagation equation suitable for studying broadband pulse evolution in optical fibers:

$$\frac{\partial A}{\partial z} - \mathrm{i}\sum_{k\geq 2}\frac{\mathrm{i}^k\beta_k}{k!}\frac{\partial^k A}{\partial t^k} = \mathrm{i}\gamma\left(1+\frac{\mathrm{i}}{\omega_0}\frac{\partial}{\partial t}\right) \times\left[A(z,t)\int_{-\infty}^{t} R(t')|A(z,t-t')|^2\mathrm{d}t'\right]. \quad (1)$$

Here, $A = A(z,t)$ is the electric field envelope, the β_ks are the usual dispersion coefficients at center frequency ω_0, $\gamma = n_2\omega_0/(cA_{\mathrm{eff}})$ is the nonlinear coefficient, with

✉ Fax: +49 711/6855097, E-mail: tuerke@iap.uni-bonn.de

$n_2 \simeq 3.0 \times 10^{-20}\,\mathrm{m}^2/\mathrm{W}$ being the nonlinear refractive index, and A_{eff} the fiber effective area. The right hand side of (1) models self-phase modulation, self-steepening, optical shock formation, and intrapulse Raman scattering. The response function $R(t) = (1 - f_{\mathrm{R}})\delta(t) + f_{\mathrm{R}} h_{\mathrm{R}}(t)$ includes both instantaneous electronic and delayed Raman contributions, with $f_{\mathrm{R}} = 0.18$ representing the contribution of the Raman response to the instantaneous nonlinear polarization. For h_{R}, we used the experimentally determined Raman response of silica fibers. Fiber loss was neglected. The presence of quantum noise was taken into account phenomenologically by including in the input field a noise seed of one photon per mode with random phase. The value of the dispersion and nonlinearity parameters were modeled locally along the length of the fiber through a lookup table.

We consider propagation in a fiber taper based on SMF28 fiber with a central waist region of 2 μm diameter and 50 mm length, centrally positioned relative to two untapered pigtails. The zero dispersion wavelength in the waist region is 730 nm.

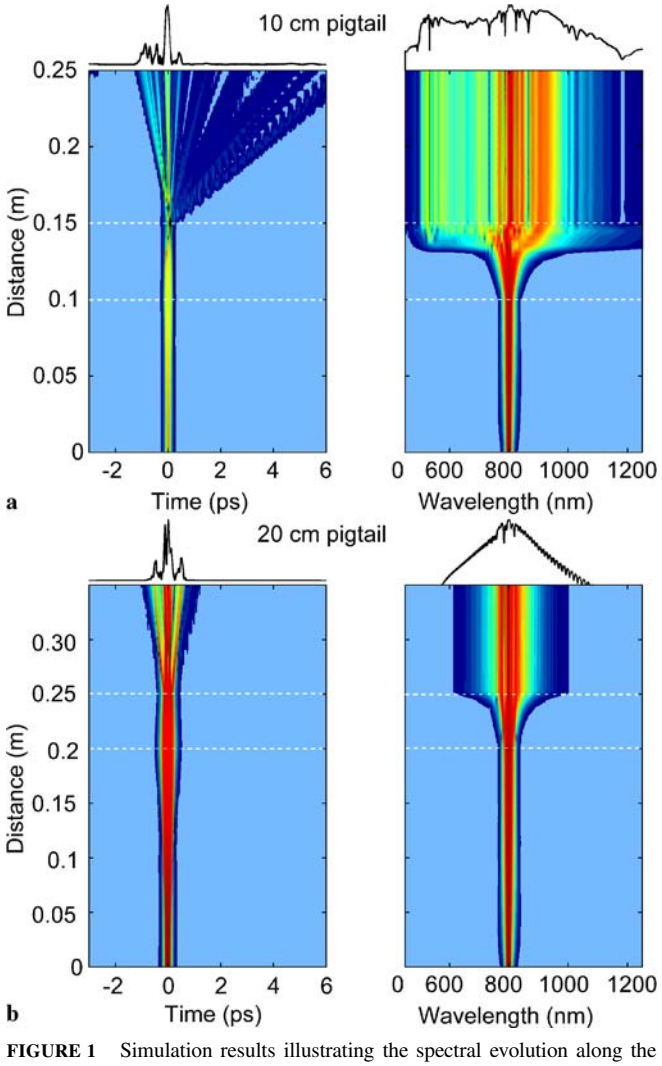

FIGURE 1 Simulation results illustrating the spectral evolution along the taper length for input pulses at 800 nm and no pre-chirp ($C = 0$) as described in the text. The *dotted lines* delineate the boundaries between the input and output pigtails and the central waist region. The false color scaling in each subfigure is independently normalized to the peak intensity during propagation

The variation of the dispersion and modal confinement in the 10 mm transition region (incorporated in the length of the pigtail) were included in the simulations but, for the parameter regime considered here, were found to have negligible influence on the qualitative behavior. To illustrate the characteristic features of the SC dynamics in tapered fibers, Fig. 1 shows simulation results for the propagation of transform-limited 120 fs input pulses (5.6 nm bandwidth) of 0.6 nJ input energy at 800 nm for different input pigtail lengths of (a) 10 cm and (b) 20 cm. The output pigtail length is 10 cm in both cases. The SC generation process is seen to occur in three phases. Propagation in the input pigtail modifies the characteristics of the pulse that is actually incident on the highly nonlinear waist region in a way that depends critically on the length of the pigtail relative to the dispersive and nonlinear lengths of the input pulse. For our pulse parameters, a 10 cm input pigtail (Fig. 1a) results in relatively minor temporal and spectral broadening of the input pulse, and the pulse incident on the waist region induces soliton fission and broadband SC generation after a distance of only 2.5 cm. In contrast, a 20 cm input pigtail (Fig. 1b) leads to significant temporal broadening (by a factor of two), and the corresponding reduction in peak power alters the propagation dynamics to such an extent that soliton fission and SC generation in the waist are effectively suppressed. In contrast to the dramatic influence of the input pigtail, the simulations reveal that the output pigtail has negligible effect on the spectral evolution after the waist, and is associated only with linear dispersive propagation and temporal walk-off of distinct spectral components.

Although these results show that propagation in a long input pigtail can completely inhibit efficient SC generation for unchirped input pulses, additional control of the soliton

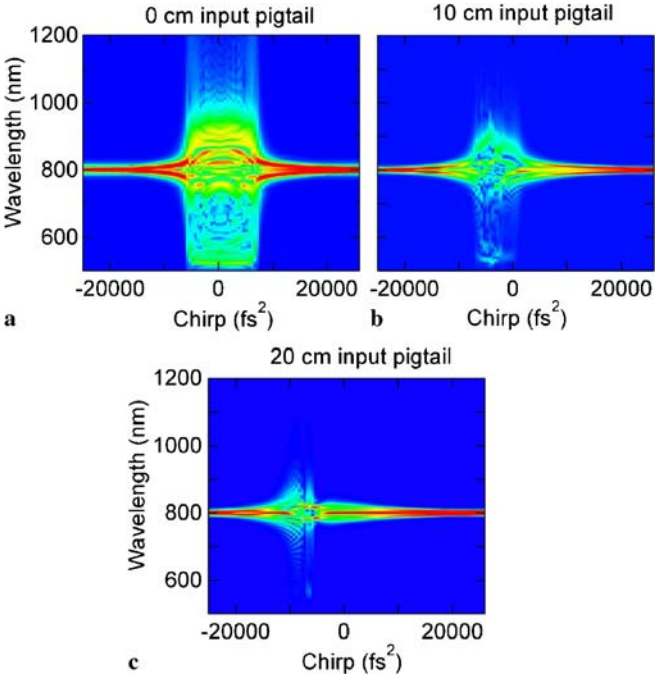

FIGURE 2 Simulation results showing the output spectrum dependence on input pre-chirp for a 2 μm taper with a 5 cm waist region, a 10 cm output pigtail, and input pigtail lengths as shown. The input pulse bandwidth is 5.6 nm

fission dynamics can be obtained by manipulating the input pulse chirp through the imposition of a quadratic spectral phase. In this case, the propagation segment in the input pigtail can be modified so that the pulse arriving at the taper waist retains sufficient peak power to induce efficient SC generation. This is seen in Fig. 2, where we present simulation results using a convenient false color representation plotting the SC spectral intensity as a function of the induced quadratic phase for differing lengths of input pigtail. The initial (unshaped) pulse in this case was again at 800 nm with 5.6 nm bandwidth. We see that, although the overall SC bandwidth decreases with increasing pigtail length, broadband SC can still be generated with relatively large 10–20 cm input pigtails by the imposition of negative pre-chirp on the input pulse. However, because of nonlinear chirp developed during propagation in the pigtail, the overall spectral bandwidths obtained are reduced for longer pigtails, and the range of initial pre-chirp that still gives substantial broadening is smaller.

3 Experiments

The expected dynamical dependence of the SC generation on input pulse pre-chirp has also been confirmed in experiments. A spatial light modulator based 4-f pulse shaper was used to impose a known quadratic spectral phase on pulses with a duration of 120 fs at center wavelengths between 750 nm and 900 nm from a Kerr-lens modelocked Ti:sapphire laser (cf. Fig. 3)[12]. We measured and recorded the experimental output spectra as a function of the imposed chirp over the range of up to 40 000 fs^2. These measurements were performed for two different input wavelengths, namely 800 and 880 nm. The key difference between these two wavelengths is the propagation in the normal and anomalous dispersion regime in the taper waist region for a waist diameter of 2.7 μm.

Figure 4 shows the calculated group velocity dispersion (GVD) parameter (in units of ps/nm/km) for a number of different fiber waist diameters. Positive GVD parameter values denote anomalous dispersion, which favors soliton formation. Figure 5a maps the output spectra for an input wavelength of 880 nm as a function of the imposed input chirp. It can be clearly seen that the spectrum broadens substantially for input chirps between −15 000 and −5000 fs^2. Larger and smaller chirps lead to only slight broadening. This slight broadening is due to self-phase modulation (SPM), whereas the large broadening is due to the soliton fission processes that occur as a result of anomalous dispersion and SPM, in combination with Raman self-frequency shift of the soliton, and simultaneous generation of nonsolitonic radiation [2, 13, 14]. The nonsolitonic part of the spectrum is visible around 650 nm. The spectral broadening is quite structured due to spectral and temporal soliton formation. To unambiguously demonstrate the presence of the temporal solitons, we set the pulse shaper pre-chirp to −8300 fs^2 and recorded the corresponding XFROG trace (cf. Fig. 5b). Temporal and spectral breakup into several solitons is visible. The overall XFROG trace has a slightly curved shape due to further dispersion in the waist and the final pigtail of the tapered fiber.

Tuning the laser to 800 nm implies propagation of the pump pulse in the normal dispersion regime. Figure 5c shows the spectral broadening as a function of input chirp, demonstrating clearly that only SPM takes place and soliton formation is absent. Figure 5d confirms this result by showing no breakup into temporal and spatial solitons. We note that the tendency of the resulting spectra, when pumping in the anomalous dispersion region, to exhibit a more structured broadening, is characteristic of the spectral evolution of the solitons [19]. We also stress that modeling this situation as shown in Fig. 2a which only includes the effect of the waist without the input pigtail, does not yield results that are in perfect agreement with the experiment, whereas the results in Fig. 2c which include the pigtail effects are qualitatively in good agreement with the experiment (cf. Fig. 5a). As the waist length in the experiment is different from the one used in the simulation, a quantitative comparison is not our aim in this case. From a practical point of view, although unchirped input pulses for this taper with a 20 cm input pigtail did not lead to significant SC generation, the imposition of negative pre-chirp of −5000 fs^2 nonetheless allows efficient SC generation to be observed with spectral broadening over 550–950 nm.

We also recorded the cartographic spectral maps for different fiber waist thicknesses. Keeping the input wavelength at 798 nm and the average input power at 180 mW, the spectral pulse breakup is substantially more pronounced for smaller waist diameters and hence higher anomalous dispersion. Figure 6 shows the cartographic spectral output as a function of input chirp, and again the soliton formation and the nonsolitonic radiation can be observed for input chirps between

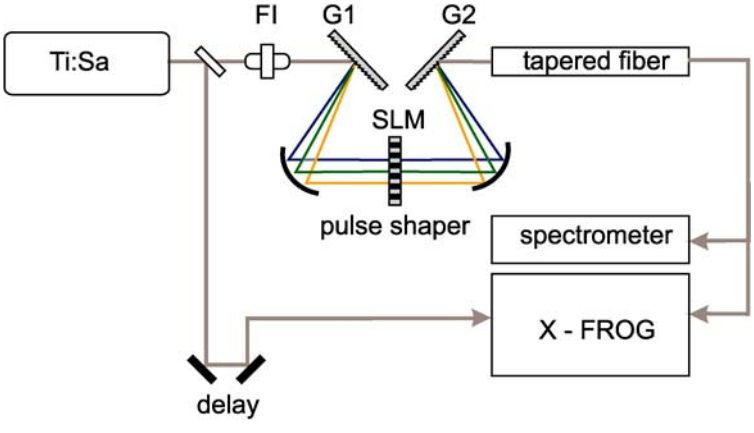

FIGURE 3 The pulses from a Ti:sapphire laser are chirped in a pulse shaper in 4-f geometry. The shaper is a grating compressor which is adjusted to zero dispersion. The shaped pulses pump a tapered fiber, and the emerging continuum is analyzed in a spectrometer and a cross correlation FROG setup, respectively. G1, G2: optical grating, SLM: spatial light modulator, FI: Faraday isolator

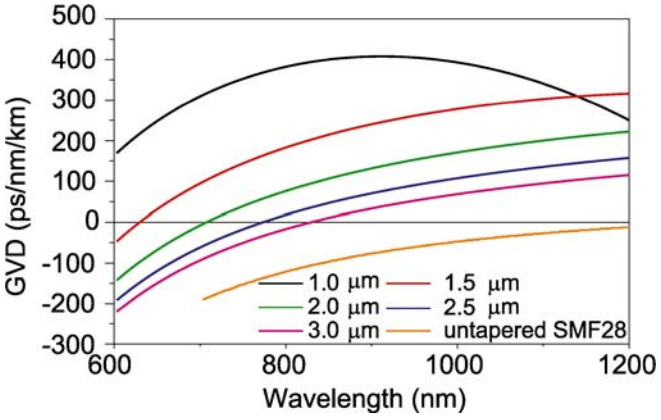

FIGURE 4 Simulated group velocity dispersion curves of an untapered SMF28 fiber and of tapered fibers with different waist diameters. Positive GVD values denote the anomalous dispersion region

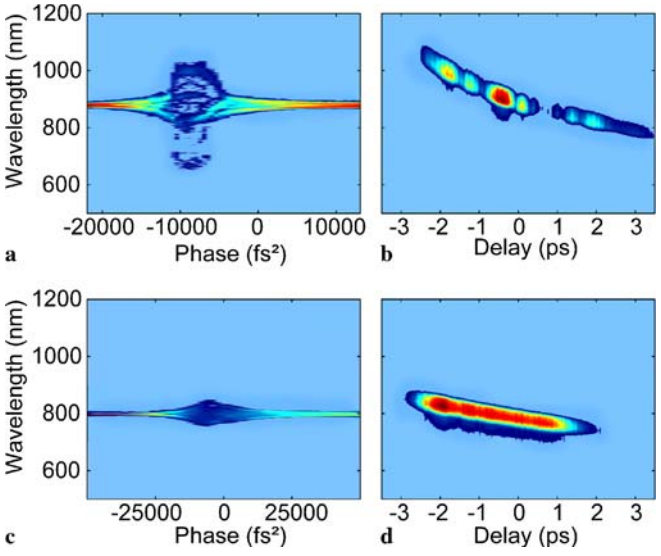

FIGURE 5 The output of the spectrometer as a function of the pre-chirp and the corresponding XFROG traces are plotted respectively for a tapered fiber with a waist diameter of 2.7 μm and a waist length of 90 mm. The average input power was 180 mW at a center wavelength of (**a**), (**b**) 880 nm (anomalous dispersion regime) and (**c**), (**d**) 798 nm (normal dispersion regime)

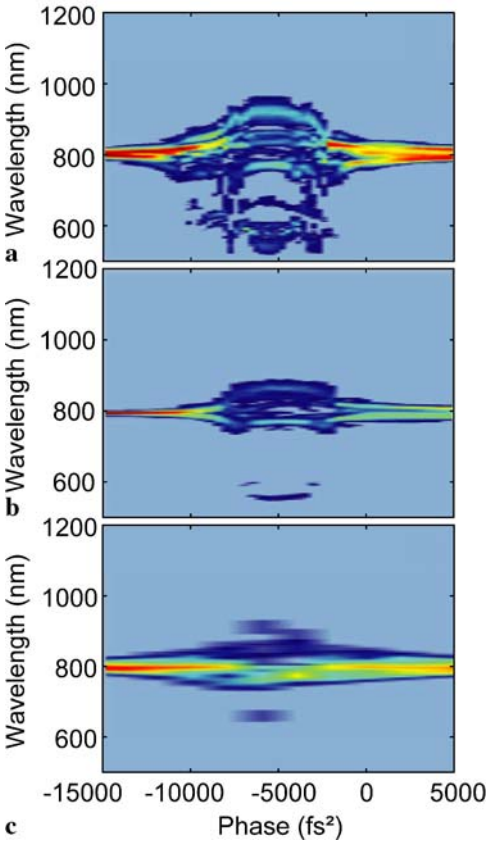

FIGURE 6 The output of the spectrometer is plotted over the pre-chirp for a tapered fiber with a waist diameter of (**a**) 1.4 μm and a waist length of 45 mm, (**b**) 2 μm and 40 mm, (**c**) 2.5 μm and 30 mm. The input power was 180 mW at a center wavelength of 798 nm

$-7500\,\mathrm{fs}^2$ and $-2000\,\mathrm{fs}^2$. Figure 6c is recorded for a waist diameter of 2.5 μm, implying a zero GVD around 800 nm, which is very close to the pump wavelength. Only for a pre-chirp of $-6000\,\mathrm{fs}^2$ is soliton formation and substantial supercontinuum generation visible, which is clear evidence that the spectral broadening is extremely dependent on the exact amount of pre-chirp. This implies that for fabrication of supercontinuum sources, fibers with smaller waist diameters should be used, giving enough anomalous dispersion and making the spectral broadening less sensitive to pre-chirp. However, a pumping wavelength closer to the zero GVD point might result in a smoother and less structured spectrum, as the comparison between Fig. 6a–c nicely demonstrates. The exact value of pre-chirp necessary to cause the maximum spectral broadening is of course dependent on the exact length of the input pigtail, which varied slightly in Fig. 6a–c. A comparison between Fig. 6b and the results in Fig. 2b shows that simulation and experiment are also quantitatively in good agreement.

Both spectra show a spectral broadening from approximately 550 nm to 900 nm at the point where the chirp of the input pigtail is completely compensated.

In order to further demonstrate the extreme sensitivity of the soliton fission process to chirp control, we recorded a series of XFROG traces for different pre-chirp settings at constant input pulse parameters for the experimental situation already discussed in Fig. 6b. By changing the input chirp from $-11\,000\,\mathrm{fs}^2$ to $-1200\,\mathrm{fs}^2$ (cf. Fig. 7) the initial conditions and thus the development of the injected higher order soliton can be controlled.

In the next series of measurements, we wanted to demonstrate how complex the dynamics of the soliton splitting and its chirp dependence can become. Figure 8a and b show the cartographic spectra as a function of input chirp for 798 nm and 180 mW input pulses, the first one for a 1.8 μm waist diameter and a 25 mm waist length, the latter one for a diameter of 2.0 μm and a waist length of 30 mm. It is interesting to observe the fan-out spectral structures for pre-chirp values of about 0 to $-2000\,\mathrm{fs}^2$. Note also the slightly asymmetric overall shape of the spectral behavior.

In order to get a detailed insight into the nonsolitonic radiation part, we carried out additional experiments using a fiber with waist diameter of 1.15 μm [15] and a waist length of 90 mm. This leads to extreme anomalous dispersion and causes a stronger blue shift in the nonsolitonic radiation. Indeed, the output of the fiber appeared very blue on visual in-

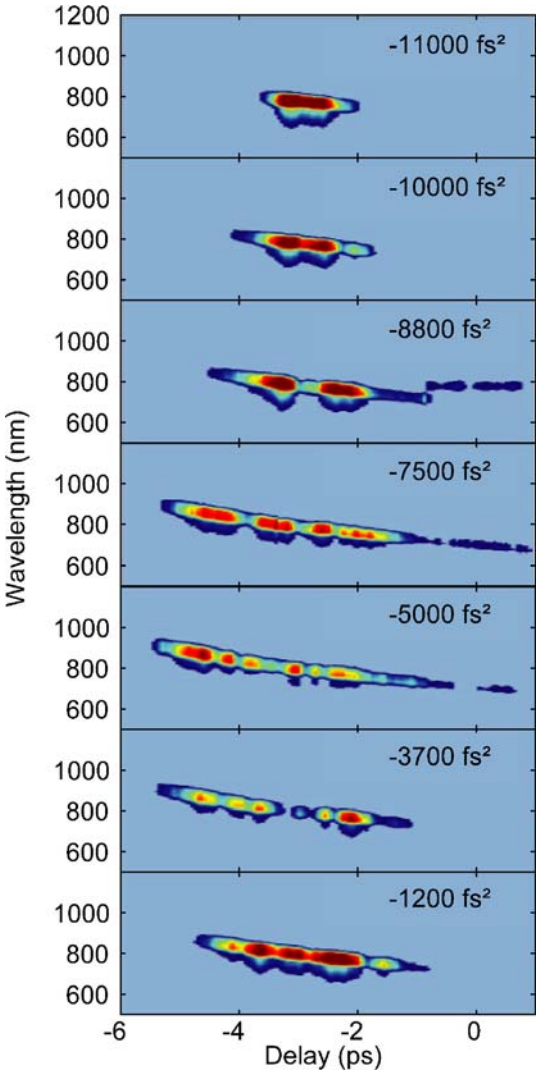

FIGURE 7 XFROG traces for different pre-chirps for a 2 μm waist diameter. The corresponding cartographic spectral output as a function of input chirp is illustrated in Fig. 6b

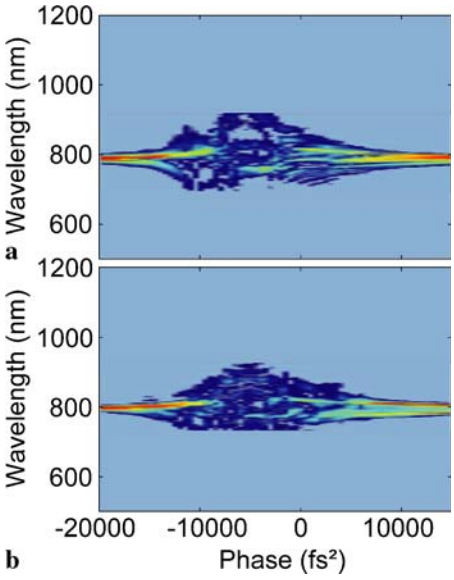

FIGURE 8 The output of the spectrometer is plotted over the quadratic prechirp for a tapered fiber with (**a**) a waist diameter of 1.8 μm and a waist length of 25 mm and (**b**) a waist diameter of 2.0 μm and a waist length of 30 mm

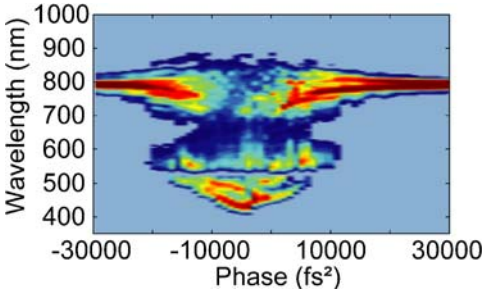

FIGURE 9 The output of the spectrometer is plotted over the quadratic prechirp for a tapered fiber with a waist diameter of 1.15 μm and a waist length of 90 mm. The diagram was taken within two runs, changing the spectrometer setting from red to blue

spection [16]. The diagram (cf. Fig. 9) nicely shows the strong nonsolitonic components for a pre-chirp around $-7000\,\mathrm{fs}^2$, which only occur when the soliton splitting is quite dramatic, and the soliton number is high (see spectral region around 800 nm). The spectral components around 600 nm are most likely the result of four-wave mixing between the solitonic and nonsolitonic spectral components [13].

4 Conclusions

There are several important conclusions to be drawn from this work. Firstly, the accurate modelling of nonlinear pulse propagation in tapers must necessarily include the effect of propagation in the pigtails in order to obtain accurate correspondence with experiment. Secondly, the use of prechirping can compensate for deleterious propagation effects in the input pigtail and allow efficient SC generation to be obtained with longer pigtails. The experimental studies show a plethora of chirp-controlled dynamics, depending on normal and anomalous dispersion, fiber thickness, waist length, and pumping wavelength. Additional XFROG measurements have demonstrated the temporal as well as spectral soliton splitting dynamics. Finally, although we have considered here only micron scale tapers, we anticipate that our conclusions will have particular significance for the optimization of nonlinear propagation effects in sub-wavelength photonic wires.

ACKNOWLEDGEMENTS Generous support by BMBF (13N8340), DFG (FOR557), K.L. Kompa and the Max-Planck-Society is gratefully acknowledged.

REFERENCES

1 A recent review of progress in the field is to be found in the Special Issue of Appl. Phys. B: Lasers and Optics **77**, 2 (2003)
2 J. Herrmann, U. Griebner, N. Zhavoronkov, A. Husakou, D. Nickel, J.C. Knight, W.J. Wadsworth, P.S.J. Russell, G. Korn, Phys. Rev. Lett. **88**, 173 901 (2003)
3 J.M. Dudley, L. Provino, N. Grossard, H. Maillotte, R.S. Windeler, B.J. Eggleton, S. Coen, J. Opt. Soc. Am. B **19**, 765 (2002)
4 K.L. Corwin, N.R. Newbury, J.M. Dudley, S. Coen, S.A. Diddams, K. Weber, R.S. Windeler, Phys. Rev. Lett. **90**, 113 904 (2003)
5 T. Uedem, J. Reichert, R. Holzwarth, T.W. Hänsch, Phys. Rev. Lett. **82** (1999)
6 B. Schenkel, Supercontinuum Generation and Compression, Ph.D. dissertation, ETH Zurich, Hartung-Gorre Verlag Series in Quantum Electronics Vol. 34 (2004)

7 B. Schenkel, R. Paschotta, U. Keller, J. Opt. Soc. Am. B **22**, 687 (2006)
8 S. Xu, D.H. Reitze, R.S. Windeler, Opt. Express **12**, 4731 (2004)
9 T.A. Birks, W.J. Wadsworth, P.S.J. Russell, Opt. Lett. **25**, 1415 (2000)
10 R. Zhang, X.P. Zhang, D. Meiser, H. Giessen, Opt. Express **12**, 5840 (2004)
11 S.G. Leon-Saval, T.A. Birks, W.J. Wadsworth, P.S.J. Russell, M.W. Mason, Opt. Expr. **12**, 2864 (2004)
12 D. Zeidler, T. Hornung, D. Proch, M. Motzkus, Appl. Phys. B **70**, 125 (2000)
13 G. Genty, M. Lethonen, H. Ludvigsen, J. Broeng, M. Kaivola, Opt. Express **10**, 1083 (2002)
14 L. Tartara, I. Christiani, V. Degiorgio, Appl. Phys. B **77**, 307 (2003)
15 F. Warken, H. Giessen, Opt. Lett. **29**, 1727 (2004)
16 J. Teipel, K. Franke, D. Tuerke, F. Warken, D. Meiser, M. Leuschner, H. Giessen, Appl. Phys. B **77**, 245 (2003)
17 S. Linden, H. Giessen, J. Kuhl, Phys. Status Solidi B **206**, 119 (1998)
18 R. Trebino, *Frequency-Resolved Optical Gating* (Kluwer Academic, Boston, 2000), Chapt. 16
19 A.V. Husakou, J. Herrmann, Phys. Rev. Lett. **87**, 203 901-1 (2002)